Mesoscience & Nanotechnology

DOI: 10.64214/jmsn.01.04001 Article

Unconventional symmetry of vortex core in Abrikosov lattice for systems with anisotropic Fermi surface

A. V. Kornev,[1] V. D. Neverov,[1,2,3] A. V. Krasavin,[1,2,3] V. S. Stolyarov[1]

[1] Moscow Institute of Physics and Technology, Dolgoprudny, Russia
[2] National Research Nuclear University MEPhI, Moscow, Russia
[3] National Research University Higher School of Economics (HSE University), Moscow, Russia

submitted 07 June 2026, accepted 05 September 2026, published 10 September 2026

We present microscopic calculations of fourfold-shaped Abrikosov vortices arising in a square crystal lattice. By solving the Bogoliubov–de Gennes equations, we demonstrate that as the Fermi surface is tuned from circular to square-like via the chemical potential, the Caroli–de Gennes–Matricon vortex-core states evolve from radially symmetric profiles into a pronounced fourfold-shaped pattern. We additionally reveal a simultaneous presence of C_4 symmetry from the Fermi surface and C_6 symmetry from the Abrikosov lattice. As a result, we anticipate unconventional symmetry features in the spatial pattern of zero-bias conductance in materials with anisotropic Fermi surfaces.

Introduction

The inner structure of Abrikosov vortices is characterized by the presence of localized quasiparticle bound states. These states were first predicted by Caroli, de Gennes and Matricon (CdGM) as a discrete set of low-energy excitations confined within the vortex core, with a characteristic energy spacing of the order Δ^2/E_F, where Δ is the superconducting gap and E_F is the Fermi energy.[1] The lowest-energy CdGM states are localized near the vortex center, while higher-energy states extend progressively farther into the surrounding superconducting region. These bound states determine the local density of states (LDOS) inside the vortex core and play a crucial role in the low-temperature electronic properties of superconductors.

Vortex bound states are of considerable interest for understanding conventional superconductivity and for interpreting vortex-core spectroscopy in candidate topological materials.[2] In topological superconductors, vortices may additionally host zero-energy Majorana bound states,[3] and candidate signatures have been reported in several systems.[4–6] The present work focuses on conventional CdGM states, whose detailed spatial structure provides an essential reference for distinguishing different low-energy vortex-core excitations. More generally, the spatial structure of the CdGM states can serve as a sensitive probe of the electronic structure of a superconductor, allowing vortices to act as localized spectroscopic detectors of the behavior of quasiparticles.[7–10]

In the simplest case of an isotropic Fermi surface and an isotropic superconducting gap, the vortex core states are expected to be radially symmetric, forming concentric ring-like LDOS patterns around the vortex center. Nevertheless, experiments have demonstrated[8,9,11] that in many real materials vortex cores frequently exhibit a pronounced spatial anisotropy that reflects the underlying electronic structure. Scanning tunneling microscopy studies have revealed vortex bound states with sixfold, fourfold, or twofold spatial symmetry, depending on the material under study. Sixfold-symmetric vortex cores have been observed in superconductors with triangular vortex lattices.[12] Twofold-symmetric vortex cores have been reported in materials with strong electronic anisotropy or nematic order.[13] Fourfold-symmetric vortex bound states have been extensively observed in systems with underlying square lattice symmetry, including iron-based superconductors.[14]

Several mechanisms can lead to anisotropic vortex core states. These include anisotropy of the superconducting gap,[15,16] anisotropy of the Fermi surface,[16] and interactions between neighboring vortices in a vortex lattice.[17] Among these effects, anisotropy of the Fermi surface is especially essential since it directly reflects the symmetry of the crystal lattice and determines the angular distribution of the quasiparticle velocities. Quasiparticles tend to propagate preferentially along directions with large Fermi velocity or low Fermi surface curvature, imprinting the Fermi surface symmetry onto the spatial structure of the CdGM states. Theoretical studies based on quasiclassical and the Bogoliubov–de Gennes approaches have shown[16,18,19] that Fermi surface anisotropy alone can produce strongly anisotropic vortex cores, even for an isotropic superconducting gap.

In addition to single-vortex properties, the geometry of the vortex lattice can influence the vortex core states when the vortices are sufficiently close.[17,20,21] While the vortex lattice is often triangular due to isotropic intervortex interactions, experiments indicate that vortices with intrinsic fourfold symmetry can exist within a triangular vortex lattice. This situation has been observed in several iron-based superconductors, where the electronic structure enforces fourfold anisotropy, while the vortex lattice remains triangular under applied magnetic fields.[12,14] The interplay between the intrinsic anisotropy of individual vortex cores and the vortex lattice geometry remains an open theoretical problem. In the effective setting considered below, the two symmetries originate from different constituents: an isotropic bulk superconductor supplies the vortex configuration, while a thin square-lattice conducting layer supplies the anisotropic dispersion.

In this work, we theoretically investigate the local density of states around an Abrikosov vortex in such a square-lattice conducting layer, both for an isolated vortex and for a triangular vortex lattice supplied by the bulk superconductor. We focus on the role of Fermi surface anisotropy and vortex–vortex interactions in shaping the spatial structure of CdGM states. The problem is studied by numerically solving the Bogoliubov–de Gennes equations for different types and strengths of Fermi surface anisotropy. Our results clarify the conditions under which the fourfold symmetry of the vortex core states is preserved or modified by the surrounding triangular vortex lattice, providing insight into recent scanning tunneling microscopy experiments on anisotropic vortices in iron-based superconductors.

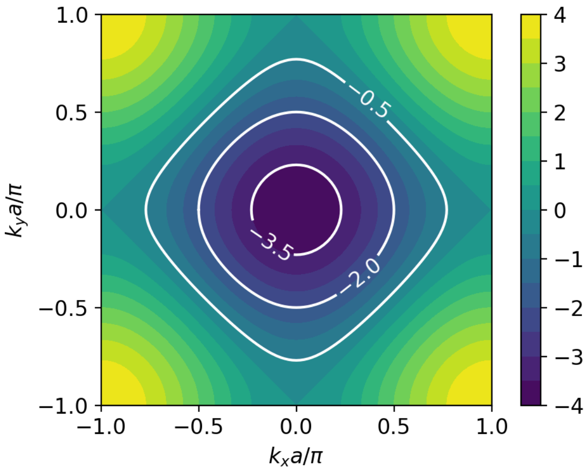

Figure 1. Fermi surfaces within the first Brillouin zone for various chemical potential values, illustrating the evolution from a circular-like to a more square-shaped surface.

Model

The calculations are done for a thin conducting layer with a square-lattice tight-binding spectrum coupled by single-particle tunneling to a macroscopically thick isotropic bulk s-wave superconductor. The total Hamiltonian of the combined system can be written as

$$\hat{\mathcal{H}}_{\rm tot} = \begin{pmatrix} \hat{\mathcal{H}} & \hat{t}_{12} \\ \hat{t}_{12}^{\dagger} & \hat{\mathcal{H}}_b \end{pmatrix}, \tag{1}$$

where $\hat{\mathcal{H}}$ and $\hat{\mathcal{H}}_b$ correspond to the conducting layer and the bulk superconductor, respectively, while the off-diagonal blocks describe tunneling through the interface with a characteristic amplitude t_{12}.

The Green function of the conducting layer is defined by

$$G^{-1}(\omega_n) = i\omega_n - \hat{\mathcal{H}} - \hat{t}_{12}\big(i\omega_n - \hat{\mathcal{H}}_b\big)^{-1}\hat{t}_{12}^{\dagger}, \tag{2}$$

where ω_n is the Matsubara frequency. The last term describes the superconducting proximity effect produced by the bulk superconductor. Its anomalous part is proportional to $|t_{12}|^2 F_b(\mathbf{r}_i, \mathbf{r}_i; \omega_n)$, where F_b is the anomalous Green function of the bulk superconductor. For the low-energy subgap states considered here, the leading contribution of this term can be represented by the induced pair potential Δ_i entering the effective Hamiltonian below.

We assume that the interface is sufficiently transparent to produce an appreciable superconducting proximity effect, while the conducting layer is sufficiently thin and its coupling to the much thicker bulk superconductor is sufficiently weak that the bulk vortex structure remains essentially unchanged. In the tunneling model, the coupling through the interface is characterized by t_{12}. Under these conditions, Δ_i inherits, to a good approximation, the phase winding, spatial profile, and symmetry of the bulk superconducting state, while its magnitude is set by the strength of the proximity effect.

The effective Hamiltonian used in the calculations is

$$H = -\sum_{ij\sigma} t_{ij} c_{i\sigma}^{\dagger} c_{j\sigma} + \sum_i \Delta_i c_{i\uparrow}^{\dagger} c_{i\downarrow}^{\dagger} - \\ - \sum_i \Delta_i^{*} c_{i\downarrow} c_{i\uparrow} - \mu \sum_{i\sigma} n_{i\sigma}. \tag{3}$$

Here $c_{i\sigma}^{\dagger}$ ($c_{i\sigma}$) are electron creation (annihilation) operators with spin σ at lattice site i, $n_{i\sigma} = c_{i\sigma}^{\dagger} c_{i\sigma}$ is the particle number operator, μ is the chemical potential, Δ_i is the pair potential induced by the bulk superconductor, and t_{ij} is the tunneling amplitude between sites i and j, which, together with μ, gives rise to a nontrivial Fermi surface.

In the Bogoliubov–de Gennes (BdG) approach, the solution to the Hamiltonian is reduced to the solution of BdG equations[22, 23]

$$\begin{pmatrix} \hat{H} - \mu & \hat{\Delta} \\ \hat{\Delta}^{*} & -\hat{H}^{*} + \mu \end{pmatrix} \begin{pmatrix} u \\ v \end{pmatrix} = E \begin{pmatrix} u \\ v \end{pmatrix}, \tag{4}$$

where $\Delta_{ij} = \Delta_i \delta_{ij}$, and the single-particle Hamiltonian $\hat{H}$ has the matrix elements

$$H_{ij} = -t_{ij}. \tag{5}$$

In our numerical calculations, we considered the simplest case of nearest neighbors with

$$t_{ij} = t e^{i\chi_{ij}}, \tag{6}$$

when the lattice sites i and j are nearest neighbors. We assume the Landau gauge in which the Peierls phase $\chi_{ij} = 0$ if the sites i and j are neighbors along the x axis, and $\chi_{ij} = \pm\pi n(x_i - x_0)/a$ if $y_i - y_j = \pm a$, $n = \Phi/\Phi_0$ is the number of quanta of magnetic flux through the unit cell.

We vary the chemical potential μ to achieve the transition from radial to C_4 symmetry. The corresponding Fermi surfaces for $\mu = -0.5t, -2.0t$ and $-3.5t$ are shown in figure 1.

For an isolated vortex, the pair potential inherited from the isotropic bulk superconductor is approximated by the radial profile

$$\Delta_i = \Delta_0 e^{i\theta_i} \tanh\left(\frac{|\mathbf{r}_i - \mathbf{r}_0|}{\xi}\right), \quad (7)$$

where Δ_0 represents the magnitude of the homogeneous gap, $|\mathbf{r}_i - \mathbf{r}_0|$ is the distance from the center of the vortex, ξ denotes the coherence length, and θ_i is the polar angle at the lattice site i. Although the leading pair-potential profile inherited from the bulk superconductor is radially symmetric, the LDOS of the vortex core follows the symmetry of the underlying Fermi surface. This symmetry breaking can be directly observed in the zero-bias conductance (ZBC) measurements.

The square-lattice quasiparticle dispersion can generate a fourfold correction to the local pair amplitude $\langle c_{i\downarrow} c_{i\uparrow}\rangle$ in the thin layer. In a complete self-consistent treatment, the inverse proximity effect can also modify the bulk vortex profile and produce quantitative changes in the core size, the CdGM energies, and the LDOS intensities. For a thin conducting layer coupled to a much thicker isotropic superconductor, the bulk profile is expected to provide the leading approximation used here.

For the multi-vortex calculation, we assume that the isotropic bulk superconductor is in a field and temperature range where a triangular Abrikosov lattice is stable. Its Ginzburg–Landau solution,[24] written in terms of the Jacobi theta function,[25] is used for Δ_i,

$$\Delta_i = C \exp\left(-\frac{\pi}{S}(x_i - x_0)^2\right) \vartheta\left(\frac{x_i + iy_i}{id} + \frac{\tau - 1}{2}\middle|\tau\right), \quad (8)$$

where C provides normalization to the magnitude of the homogeneous gap Δ_0, d denotes the spacing between vortices in the Abrikosov lattice and $\tau = e^{i\pi/3}$ represents the symmetry factor. The Jacobi theta function is defined by the expression

$$\vartheta(z|\tau) = \sum_{n=-\infty}^{\infty} \exp\left(\pi i n^2 \tau + 2\pi i n z\right). \quad (9)$$

The solution (8) is consistent with the choice of the Landau gauge when determining the Peierls phases in Eq. (6) with $x_0 = \sqrt{3}/(4d)$, $n = \Phi/\Phi_0 = a^2/S$, $S = \sqrt{3}/(2d^2)$, and S is an area of the vortex lattice unit cell containing one quantum of magnetic flux.

The triangular lattice supplied by the thick isotropic bulk superconductor can provide a good approximation to the self-consistent vortex configuration of the complete heterostructure when the bulk contribution dominates the vortex-lattice free energy. In a single-component fourfold-anisotropic superconductor, or when the influence of the conducting layer on the bulk condensate is appreciable, the equilibrium vortex lattice can instead become rhombic or square.[16,26] The results below apply to the case where the thin layer produces only a small anisotropic correction to the vortex configuration.

For numerical calculations, we use $\Delta_0 = 0.1t$ and $\xi = 10a$, where a is the lattice constant. The size of the lattice reaches values up to $200a \times 200a$, which is much larger than the characteristic size of the vortex. The BdG equations (4) can be solved using various approaches, including exact diagonalization,[27] kernel polynomial methods,[28] and even machine learning techniques.[29,30] To calculate the local density of states in the vicinity of the vortex core, we employ the Chebyshev–Bogoliubov–de Gennes approach,[28] a kernel polynomial technique that enables efficient treatment of large system sizes.

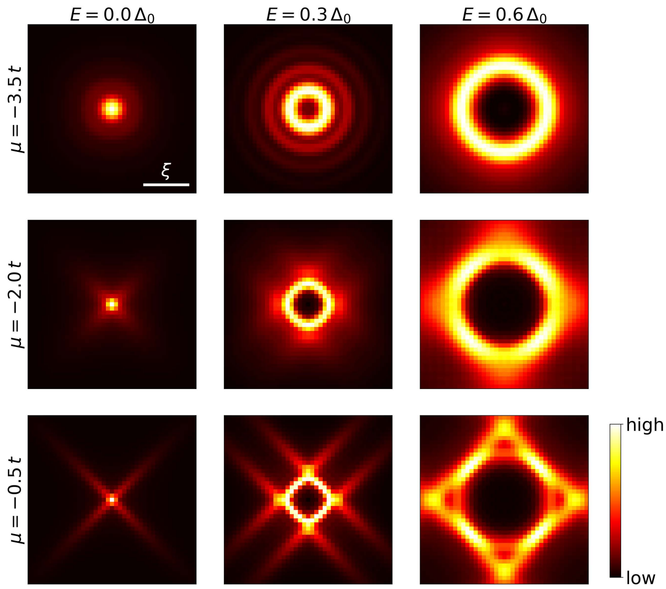

Figure 2. LDOS in the vicinity of a vortex for different values of the chemical potential μ, illustrating the evolution from a circular to a more square-shaped Fermi surface at several energies. Here, ξ denotes the coherence length, and Δ_0 represents the magnitude of the uniform gap.

Results

In order to show the transition from the radial to squarish structure of a single vortex, we calculate the local density of states according to the solution of the BdG equations (4) with a pair potential profile (7). Using this leading pair-potential profile as input, the solution of the BdG equations yields the LDOS near the vortex center shown in figure 2.

As is well known, for a circular Fermi surface ($\mu = -3.5t$), the vortex core states exhibit the radially symmetric structure predicted by CdGM theory.[1] Their energy spectrum is given by $E_m = m\Delta^2/E_F$, with half-integer angular momentum quantum numbers $m = \pm 1/2, \pm 3/2, \pm 5/2, \ldots$. The lowest-energy states are tightly bound to the vortex center, while higher-energy states extend progressively outward.

When the Fermi surface becomes squarish ($\mu = -2.0t$), the vortex states develop a clear fourfold symmetry, yet the same energy-dependent spatial structure persists: low-energy states remain concentrated near the core, and higher-energy states appear at larger distances. Intermediate chemical potentials merely enhance the squarish shape without altering this trend. In the extreme case $\mu = -0.5t$ the anisotropy becomes strongly pronounced. The low-energy states are aligned with the diagonal di-

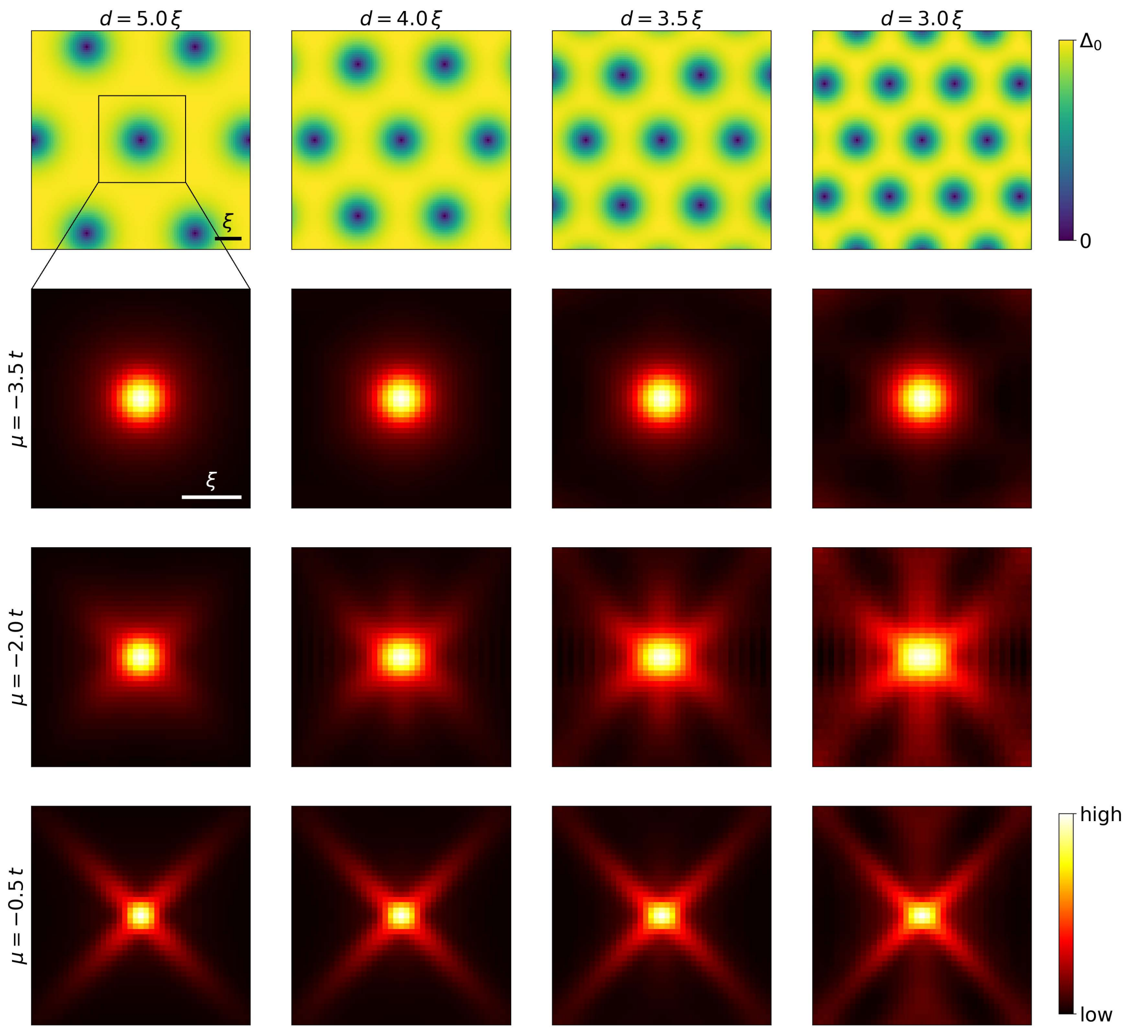

Figure 3. Zero-bias conductance (LDOS at $E = 0$) in the vicinity of a vortex within a triangular Abrikosov lattice, shown for various intervortex spacings d and different Fermi surfaces (set by μ). Here, ξ denotes the coherence length and t is the hopping amplitude.

rections, producing a four-leaf pattern in the LDOS at zero energy that is directly visible in ZBC maps.

The Fermi surface anisotropy is not the only mechanism that can reshape the CdGM bound states. We next consider the triangular Abrikosov lattice supplied by the isotropic bulk superconductor. As the lattice constant d decreases, neighboring vortices become close enough to influence the core states of each other. To investigate this effect, we compute the LDOS near a vortex embedded in an Abrikosov lattice, scanning both lattice constant d and different Fermi surface shapes controlled by the chemical potential μ. The results are summarized in figure 3. The upper panel displays the pairing potential ansatz for various d obtained from Eq. (8). The lower panels present the corresponding near zero energy LDOS for the central vortex, revealing how the vortex core structure evolves with d and μ.

For the circular Fermi surface ($\mu = -3.5t$), the vortex core states remain nearly unchanged as the vortex lattice constant d decreases. In practice, vortices have to approach each other extremely closely before the radial symmetry of the CdGM states becomes disturbed.

In contrast, an intermediate value of the chemical potential ($\mu = -2.0t$) reveals a nontrivial evolution of the vortex core symmetry upon vortex approach. For large $d = 5\xi$, the vortex state is identical to the one of isolated vortex shown in figure 2. However, as d becomes smaller, the influence of the sixfold symmetry originating from the surrounding triangular Abrikosov lattice grows comparable to the influence of the intrinsic fourfold symmetry of the vortex core. This interplay gives rise to a six-leaf pattern in the local density of states at low energies. Strictly speaking, this is not a perfect sixfold symmetry because the leaves are not equivalent. The inequivalence becomes even more pronounced for the extreme Fermi surface anisotropy ($\mu = -0.5t$), where the contributions arising from the intrinsic Fermi surface anisotropy versus those induced by the vortex lattice geometry can be clearly distinguished. Accordingly, within the field and temperature range where the bulk vortex lattice remains triangular, for systems possessing a roughly square Fermi surface, we anticipate a change in the vortex core structure as the external magnetic field is raised and the resulting vortex density increases. This evolution should be directly observable in ZBC measurements.

Finally, we investigate the near zero-energy LDOS

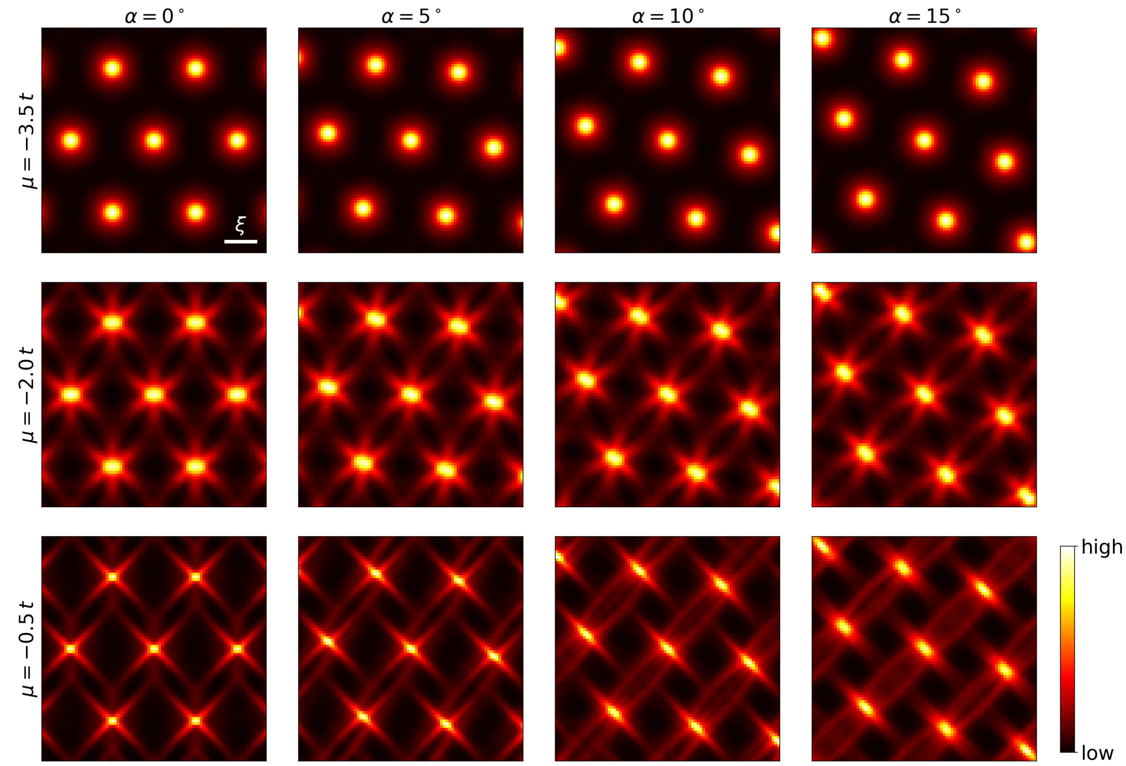

Figure 4. Zero-bias conductance (LDOS at $E = 0$) shown for various rotation angles α of the Abrikosov triangular vortex lattice with respect to the square crystal lattice and the Fermi surfaces (different values of μ). Here, ξ denotes the coherence length and t is the hopping amplitude.

profile as a function of the relative orientation between the crystal lattice and the vortex lattice. In real samples, the angle between the crystallographic axes and the Abrikosov vortex lattice can vary due to sample imperfections and vortex pinning. In figure 4 we present the spatial LDOS profiles for different rotation angles between the two lattices.

In the heterostructure considered here, the relative orientation can be selected by weak interfacial anisotropy, sample boundaries, defects, or vortex pinning. Figure 4 therefore presents the electronic response for prescribed symmetry-inequivalent orientations. The equilibrium value of α is material- and geometry-dependent and requires a separate calculation of the total free energy.

The combined C_4 and C_6 rotational symmetries make the relative orientation periodic under a rotation of 30 degrees, while mirror symmetry identifies α with $-\alpha$. Therefore, we show results for angles from 0 to 15 degrees, which capture all symmetry-inequivalent configurations.

Figure 4 reveals how the system transforms as the angle of misalignment increases. For the circular Fermi surface ($\mu = -3.5t$), the vortex core remains isotropic and unchanged, as expected. In sharp contrast, for intermediate ($\mu = -2.0t$) and extreme ($\mu = -0.5t$) values, which correspond to squarish Fermi surfaces, the system develops a pronounced twofold symmetry. The four-leaf pattern progressively deforms and, when the misalignment angle reaches 15 degrees, the LDOS becomes markedly stretched along one of the diagonals. This crossover from fourfold to twofold symmetry arises from the interplay between the intrinsic fourfold anisotropy of the vortex core and the sixfold symmetric potential of the surrounding vortex lattice. When the two lattices are misaligned, the superposition no longer preserves the original fourfold or sixfold axes, and a lower twofold symmetry emerges.

Conclusion

We have investigated the structure of Abrikosov vortex cores in a thin square-lattice conducting layer proximity-coupled to a macroscopically thick isotropic bulk s-wave superconductor. Our focus is on the interplay between the intrinsic fourfold anisotropy of the core and the sixfold symmetry imposed by a triangular vortex lattice. By solving the Bogoliubov–de Gennes equations, we determine that a single isolated vortex supports fourfold-shaped CdGM states, while a dense triangular vortex lattice superimposes an additional sixfold symmetry on the system. A misalignment between the crystal axes and the vortex lattice leads to a twofold elongation of the zero-bias conductance pattern.

Our calculations use an effective description in which the superconducting state of the conducting layer is determined by the nearby bulk superconductor. We retain the induced pair potential at each lattice site, while changes in the normal electronic spectrum are included in the effective hopping amplitudes t_{ij} and chemical potential μ. The vortex profile is taken to be radially symmetric, and the many-vortex calculations assume a triangular Abrikosov lattice. These assumptions are appropriate for a thin conducting layer coupled to a much thicker isotropic bulk superconductor whose contribution dominates the vortex shape and the vortex-lattice structure.

A more complete calculation, in which the two constituents influence each other, could introduce a fourfold correction to the pair amplitude and quantitatively change the vortex-core size, the CdGM energies, and the LDOS intensities. If the conducting layer strongly affects the bulk superconductor, if the bulk superconductor is sufficiently thin, or if the superconducting constituent itself has pronounced fourfold anisotropy, the vortex lattice may become rhombic or square and the sixfold features discussed here may be weakened. The calculations also assume a clean ideal system and prescribed relative orientations. Disorder, pinning, sample boundaries, and interface anisotropy may modify the detailed LDOS patterns and select the equilibrium orientation. Under these assumptions, our results provide qualitative predictions for systems in which an anisotropic quasiparticle spectrum coexists with a triangular vortex lattice determined by the bulk superconductor.

Acknowledgements

This work is supported by the Russian Science Foundation (project 23-72-30004). Authors thank Prof. S. Pan for useful discussions.

Contact information

Corresponding author: A. V. Kornev,
orcid.org/0009-0000-2381-2798,
e-mail: art.kor.new@yandex.ru

References

[1] Caroli C., de Gennes P. G., Matricon J. *Bound Fermion states on a vortex line in a type II superconductor.* Phys. Rev. Lett., vol. 9, 307–309 (1964).

[2] Beenakker C. W. J. *Search for Majorana Fermions in Superconductors.* Annu. Rev. Condens. Matter Phys., vol. 4, 113–136 (2013).

[3] Sato M., Ando Y. *Topological superconductors: a review.* Rep. Prog. Phys., vol. 80, 076501 (2017).

[4] Mourik V., Zuo K., Frolov S. M., Plissard S. R., Bakkers E. P. A. M., Kouwenhoven L. P. *Signatures of Majorana Fermions in Hybrid Superconductor-Semiconductor Nanowire Devices.* Science, vol. 336, 1003–1007 (2012).

[5] Nadj-Perge S., Drozdov I. K., Li J., Chen H., Jeon S., Seo J., MacDonald A. H., Bernevig B. A., Yazdani A. *Observation of Majorana fermions in ferromagnetic atomic chains on a superconductor.* Science, vol. 346, 602–607 (2014).

[6] Wang D., Kong L., Fan P., Chen H., Zhu S., Liu W., Cao L., Sun Y., Du S., Schneeloch J., Zhong R., Gu G., Fu L., Ding H. *Evidence for Majorana bound states in an iron-based superconductor.* Science, vol. 362, 333–335 (2018).

[7] Fischer Ø., Kugler M., Maggio-Aprile I., Berthod C., Renner C. *Scanning tunneling spectroscopy of high-temperature superconductors.* Rev. Mod. Phys., vol. 79, 353–419 (2007).

[8] Hess H. F., Robinson R. B., Dynes R. C., Valles J. M. Jr., Waszczak J. V. *Scanning-Tunneling-Microscope Observation of the Abrikosov Flux Lattice and the Density of States near and inside a Fluxoid.* Phys. Rev. Lett., vol. 62, 214–216 (1989).

[9] Hess H. F., Robinson R. B., Waszczak J. V. *Vortex-core structure observed with a scanning tunneling microscope.* Phys. Rev. Lett., vol. 64, 2711–2714 (1990).

[10] Stolyarov V. S., Neverov V., Krasavin A. V., Kasatonov D. I., Panov D., Baranov D., Skryabina O. V., Melnikov A. S., Golubov A. A., Kupriyanov M. Yu., Shanenko A. A., Cren T., Aladyshkin A. Yu., Vagov A., Roditchev D. *Microscopic structure of the vortex cores in granular niobium: A coherent quantum puzzle.* ArXiv 2601.20486 (2026).

[11] Guillamón I., Suderow H., Vieira S., Cario L., Diener P., Rodière P. *Superconducting Density of States and Vortex Cores of 2H-NbSe$_2$.* Phys. Rev. Lett., vol. 101, 166407 (2008).

[12] Suderow H., Guillamón I., Rodrigo J. G., Vieira S. *Imaging superconducting vortex cores and lattices with scanning tunneling microscope.* Supercond. Sci. Technol., vol. 27, 063001 (2014).

[13] Fan Q., Zhang W. H., Liu X., Yan Y. J., Ren M. Q.,. Xia M, Chen H. Y., Xu D. F., Ye Z. R., Jiao W. H., Cao G. H., Xie B. P., Zhang T., Feng D. L. *Scanning tunneling microscopy study of superconductivity, magnetic vortices, and possible charge-density wave in $Ta_4Pd_3Te_{16}$.* Phys. Rev. B, vol. 91, 104506 (2015).

[14] Hanaguri T., Kitagawa K., Matsubayashi K., Mazaki Y., Uwatoko Y., Takagi H. *Scanning tunneling microscopy/spectroscopy of vortices in LiFeAs.* Phys. Rev. B, vol. 85, 214505 (2012).

[15] Vekhter I., Hirschfeld P. J., Carbotte J. P., Nicol E. J. *Anisotropic thermodynamics of d-wave superconductors in the vortex state.* Phys. Rev. B, vol. 59, R9023–R9026 (1999).

[16] Nakai N., Miranović P., Ichioka M., Machida K. *Reentrant Vortex Lattice Transformation in Fourfold Symmetric Superconductors.* Phys. Rev. Lett., vol. 89, 237004 (2002).

[17] Ichioka M., Hasegawa A., Machida K. *Vortex lattice effects on low-energy excitations in d-wave and s-wave superconductors.* Phys. Rev. B, vol. 59, 184–199 (1999).

[18] Hayashi N., Isoshima T., Ichioka M., Machida K. *Low-Lying Quasiparticle Excitations around a Vortex Core in Quantum Limit.* Phys. Rev. Lett., vol. 80, 2921–2924 (1998).

[19] Mel'nikov A. S., Samokhvalov A. V., Zubarev M. N. *Electronic structure of vortices pinned by columnar defects.* Phys. Rev. B, vol. 79, 134529 (2009).

[20] Franz M., Tešanović Z. *Self-Consistent Electronic Structure of a $d_{x^2-y^2}$ and a $d_{x^2-y^2}+id_{xy}$ Vortex.* Phys. Rev. Lett., vol. 80, 4763–4766 (1998).

[21] Franz M., Tešanović Z. *Quasiparticles in the Vortex Lattice of Unconventional Superconductors: Bloch Waves or Landau Levels?* Phys. Rev. Lett., vol. 84, 554–557 (2000).

[22] Zhu J.-X. *Bogoliubov-de Gennes Method and Its Applications.* Lecture Notes in Physic s, vol. 924, Springer (2016).

[23] de Gennes P. G. *Superconductivity of Metals and Alloys.* Boca Raton, CRC Press (2018).

[24] Kleiner W. H., Roth L. M., Autler S. H. *Bulk Solution of Ginzburg-Landau Equations for Type II Superconductors: Upper Critical Field Region.* Phys. Rev., vol. 133, A1226–A1227 (1964).

[25] Abrikosov A. A. *Fundamentals of the Theory of Metals.* Dover Publications (2017).

[26] Park K., Huse D. A. *Phase transition to a square vortex lattice in type-II superconductors with fourfold anisotropy.* Phys. Rev. B, vol. 58, 9427–9432 (1998).

[27] Ghosal A., Rabderia M., Trivedi N. *Inhomogeneous pairing in highly disordered s-wave superconductors.* Phys. Rev. B, vol. 65, 014501 (2001).

[28] Covaci L., Peeters F. M., Berciu M. *Efficient Numerical Approach to Inhomogeneous Superconductivity: The Chebyshev–Bogoliubov–de Gennes Method.* Phys. Rev. Lett., vol. 105, 167006 (2010).

[29] Neverov V., Krasavin A., Tomayeva M., Vagov A. *Machine learning prediction of superconducting pairing potential for quasi-one-dimensional disordered s-wave superconductors.* Mesosci. Nanotechnol., vol. 1, 02005 (2025).

[30] Neverov V., Lukyanov A., Krasavin A., Vagov A. *Scalable machine learning approach to disordered s-wave superconductors.* Phys. Rev. B, vol. 113, 024515 (2026).